

High Velocity Gas Outflows from H II regions in Disc Galaxies

Relaño M.^{1*}, Beckman J. E.² and Rozas M.³

¹ Instituto de Astrofísica de Canarias, C/Vía Láctea s/n, 38200 La Laguna, Tenerife, Spain

² Instituto de Astrofísica de Canarias, C/Vía Láctea s/n, 38200 La Laguna Tenerife, Spain

³ Observatorio Astronómico Nacional (UNAM), Apartado Postal 877 Ensenada, B.C., México

Abstract We analyze the H α emission line profiles of the H II region populations in three disc spiral galaxies and find evidence of wing features at 40–90 km s⁻¹ from the central peak in a significant fraction of regions. We explain the wing features as due to a shell expanding inside the H II region, quantify the energy involved and present two possible mechanisms to drive the expanding shell.

Key words: H II regions – ISM: jets and outflows – stars: mass loss

1 H II REGIONS WITH HIGH VELOCITY AND LOW INTENSITY FEATURES

We have observed a sample of three spiral galaxies NGC 1530, NGC 3359 and NGC 6951 in H α with the TAURUS Fabry-Pérot scanner on the 4.2 m WHT (La Palma). The observations consist of a scanning of the emission line H α in 55 closely spaced wavelengths steps; for the case of NGC 3359 each step is of 0.34 Å interval, corresponding to a velocity step of 15.6 km s⁻¹. The result is a data cube with 55 planes containing the emission of the galaxy at each stepped wavelength. Further details of the observational parameters for each galaxy can be found in Zurita et al. (2003) and Rozas et al. (2000, 2002) for NGC 1530, NGC 3359 and NGC 6951, respectively. The data cube allows us to obtain the total H α intensity (zereth moment), velocity (first moment) and velocity dispersion (second moment) maps. For flux calibration we compare the intensity maps with narrow-band H α photometric observations of each galaxy. Continuum-subtracted H α images are used to obtain an H II region catalogue of each galaxy; these catalogues are archives which contain the centre position, integrated H α flux, radius and local background adopted for each H II region in the galaxy. Once we have identified the catalogued H II regions in the intensity map, we use the catalogued radius to obtain the aperture which defines the H II region in the intensity map and taking it as a reference value we extract the integrated line profiles of each H II region from the Fabry-Pérot data cube. These profiles were fitted by a set of Gaussian components.

* E-mail: mpastor@ll.iac.es

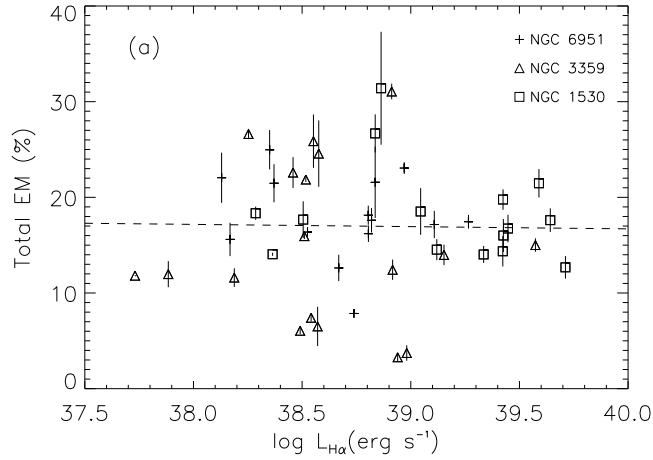


Fig. 1 Summed Emission Measure of the red and blue Gaussian components fitted to the best S:N line profiles $v. \log L_{\text{H}\alpha}$ for the H II regions showing two wing features in their line profiles. The summed EM is given as a fraction of the total EM of the H II region and the errors shown correspond to the variation of the EM in the set of line profiles taken with different apertures for each H II region. The dashed line shows the linear fit to the data.

The most striking phenomenology we found in the emission line profiles of individual H II regions was the existence of high velocity low intensity features symmetrically located at radial velocities which differ by $40\text{--}90\text{ km s}^{-1}$ from that of the central peak. We apply two criteria to the wing features to verify their existence, they are: a) the amplitudes of the secondary components must be bigger than 2.5 times the root mean square noise level¹ of the line profile and b) each secondary Gaussian component must be separated from the central one by more than 2.5 times the spectral resolution of the corresponding observed data cube². Down to a limit of $\log L_{\text{H}\alpha} = 38.0$ (ergs^{-1}), the H II regions whose line profiles show wing features satisfying the criteria defined above represent for NGC 3359, NGC 6951 and NGC 1530 respectively, 26.77%, 42.0% and 31.63% of the total identified H II regions for each galaxy, but we suspect that with improved S:N ratio these fractions would increase significantly.

2 OBSERVATIONAL PARAMETERS OF THE WING FEATURES

For the sample of H II regions with high velocity, low intensity features, we obtained line profiles with increasing apertures; starting from a line of sight through the centre of the region (line spectrum taken with an aperture of 1×1 pixel), we continued opening the aperture till we

¹ We define the root mean square noise level as the standard deviation of the points of the spectrum located in velocity axis at more than six times the velocity dispersion of the single Gaussian fitted to the line profile.

² The spectral resolution here is the velocity separation between adjacent steps. The values for the three galaxies are 15.63 km s^{-1} , 16.66 km s^{-1} and 18.62 km s^{-1} for NGC 6951, NGC 3359 and NGC 1530, respectively.

had covered the whole emitting area of the region. We studied carefully the isolation of each H II region and its set of spectra taken with different apertures to extract a more restricted sample with clear high velocity features. With this procedure we guarantee that the secondary components of the final selected sample of H II region line profiles show the emission from the given region, thus they are not contaminated by the emission of neighbouring regions. Finally, we take as the line profile that best defines the wing features from the set of line profiles for each H II region, the one with the highest *mean* S:N in its secondary components.

The relation between the summed Emission Measure of the wing features for the best S:N line profile and the logarithmic H α luminosity for the more restricted H II region sample is shown in Fig. 1. The summed EM ranges from 5%–30% of the total EM of the region, and its mean value is $\langle \text{EM}_{\text{sum}} \rangle = 17.0\%$. Figure 2 shows the *mean* velocity separation of the wing features from the central peak velocity for the same H II regions as in Fig. 1 *v. log L α* . The mean value for the velocity separation is $\langle v_{\text{mean}} \rangle = 60.4 \text{ km s}^{-1}$. There is a light trend of increasing velocity separation with increasing $\log L_{\text{H}\alpha}$, which can be seen in the linear fit plotted in dashed line in the diagram.

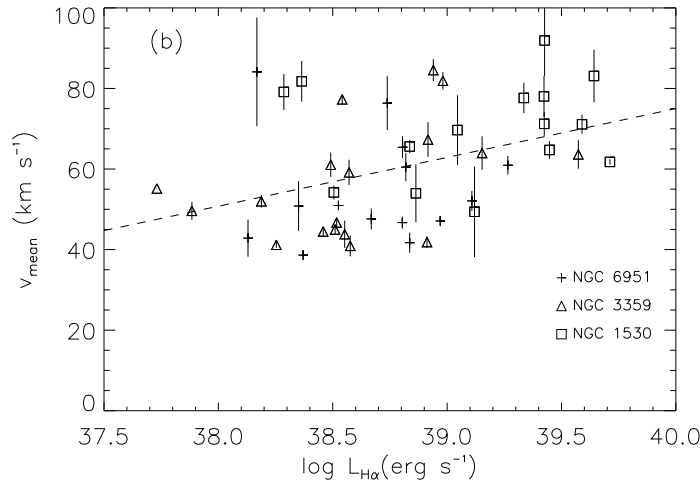


Fig. 2 Mean velocity of the red and blue Gaussian components *v. log L α* for the same H II regions as in Fig. 1. The errors shown correspond to the variation of the mean velocity in the set of line profiles taken with different apertures for each H II region. The dashed line shows the linear fit to the data.

3 ENERGETICS OF THE H II REGION SAMPLE AND THEIR EXPANDING SHELLS

The wing features are evidence of expanding gas moving inside the H II region. Since the features are located symmetrically with respect to the central component, we explain them as due to a shell expanding with a velocity which is the mean of the difference between the velocity of the feature and the central component.

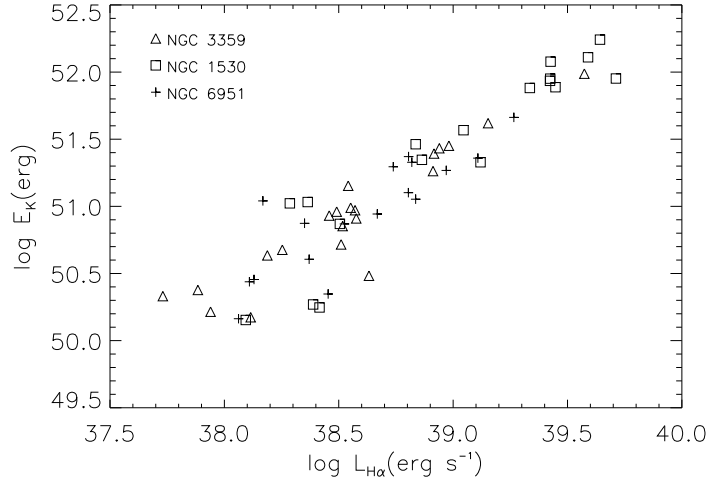


Fig. 3 Logarithmic kinetic energy of the shell *v.* logarithmic H α luminosity for the more restricted sample of H II regions in the three galaxies, NGC 1530, NGC 3359 and NGC 6951.

In Table 1, we show the parameters of the expanding shell for a selected group of H II regions of the three galaxies. The density of the shell is obtained from the ratio between the Emission Measure of the shell and the Emission Measure of the region, assuming a shell thickness of 1 pc from measurements of local H II regions (Chu & Kennicutt 1994) and a value of the r.m.s. electron density for the H II region obtained from the total Emission Measure of the region. Making an estimate of the shell radius as the half of the H II region radius we obtain the kinetic energy of the shell from $1/2 m_{\text{shell}} v_{\text{shell}}^2$. In Fig. 3 we show the relation between the kinetic energy of the shell and the luminosity of the H II region. There is a clear trend of increasing kinetic energy of the shell with increasing H α luminosity. We also compare in Table 1 the kinetic energy of the shell with the stellar wind energy input from the OB association. The stellar wind energy is estimated from the equivalent number of O3(V) type stars necessary to obtain the H α luminosity of the H II region; using the H α luminosity and the stellar wind energy input of a O3(V) type star given by Vacca et al. (1996) and Leitherer (1998), respectively. We also compute the turbulent kinetic energy of the whole region using the non-thermal velocity dispersion of the central and most intense component. For comparison we also present the ionizing radiative energy, and the integrated radiative energy input of the OB association.

4 POSSIBLE MECHANISMS

We propose two possible mechanisms to produce the expanding shell: *mass-loading winds* (Dyson et al. 1995), in which the interaction of the wind and the ionizing radiation from the OB association with the clumpy medium produce a flow with a constant volume rate of mass injection coming from the clumps, and *radiation driving with dust coupling* (Elitzur & Ivezić 2001), where dust can be accelerated by the radiation field and the linear momentum of the dust can be transferred to the gas, the result being an acceleration of the gas due to the radiation

Table 1 Energetics of the shell, the turbulent component and the input energies of a selected group of H II regions from NGC 1530, NGC 3359 and NGC 6951. Columns: 1. Region reference number; 2. Logarithmic H α luminosity (erg s^{-1}); 3. Shell radius; 4. Measured shell expansion velocity; 5. Shell Emission Measure as a fraction of the total EM of the region; 6. Mean shell electron density; 7. Kinetic energy of the shell; 8. Combined kinetic energy of OB stellar winds; 9. Turbulent kinetic energy of the H II region gas; 10. Combined energy of the ionizing radiation from the OB association; 11. Combined total radiative energy of the OB association.

Region	$\log L_{\text{H}\alpha}$ (erg s^{-1})	R_{shell} (pc)	$\langle v_{\text{shell}} \rangle$ (km s^{-1})	EM (%)	$\langle N_{\text{shell}} \rangle$ (cm^{-3})	E_{K} (10^{51}erg)	E_{wind} (10^{51}erg)	E_{turb} (10^{53}erg)	E_{rad} (10^{53}erg)	$E_{\text{total rad}}$ (10^{53}erg)
8	39.45	205.0	64.72	8.37	14.18	7.7	10.4	11.2	14.2	36.0
6	39.15	174.1	63.97	6.99	10.87	4.2	5.3	3.2	7.2	18.3
4	39.11	137.0	52.08	8.58	8.58	2.3	4.8	1.7	6.5	16.5
33	38.86	121.4	53.98	15.7	16.75	2.2	2.7	1.2	3.7	9.4
51	38.52	92.9	46.73	10.93	12.26	0.7	1.2	0.02	1.7	4.2
24	38.52	92.9	50.95	10.71	8.19	0.7	1.2	0.2	1.7	4.3

of the star cluster. Both mechanisms supply reasonable energy contributions, since the stellar wind energy and the ionizing radiative energy are higher than the kinetic energy of the shell, as it is shown in Table 1, though the coupling efficiencies of both mechanisms are significantly less than unity.

References

- Chu, Y. -H., Kennicutt, R. C., 1994, ApJ, 425, 720
Dyson, J. E., Williams, R. J. R., Redman, M. P., 1995, MNRAS, 277, 700
Elitzur, M., Ivezić, Ž., 2001, MNRAS, 327, 403
Leitherer, C., 1998, In: Aparicio, A., Herrero, A., F. Sánchez, eds., Cambridge: Cambridge University Press, Populations of Massive Stars and the Interstellar Medium, p. 527
Rozas, M. Relaño, M., Zurita, A., Beckman, J. E., 2002, A&A, 386, 42
Rozas, M., Zurita, A., Beckman, J. E., 2000, A&A, 354, 823
Vacca, W.D., Garmany, C. D., Shull, M., 1996, ApJ, 460, 914
Zurita, A., Relaño, M., Beckman, J.E., Knapen, J.H., 2003, A&A, in press (astro-ph/0307234)